Structure and Thermal Properties of the Nonlinear Optical Crystal BaTeMo 2 O 9

ARTICLE *in* CRYSTAL GROWTH & DESIGN · JUNE 2009

Impact Factor: 4.89 · DOI: 10.1021/cg8011052

CRYSTAL GROWTH & DESIGN
2009
VOL. 9, NO. 6
2633–2636

Structure and Thermal Properties of the Nonlinear Optical Crystal $BaTeMo_2O_9$

Weiguo Zhang, Xutang Tao,* Chengqian Zhang, Huaijin Zhang, and Minhua Jiang

State Key Laboratory of Crystal Materials, Shandong University, Jinan, 250100, China

Received October 2, 2008; Revised Manuscript Received March 5, 2009

ABSTRACT: Nonlinear optical (NLO) crystals $BaTeMo_2O_9$ (BTM) with large size and good quality have been grown by the flux method. The connections of the Mo−O octahedral group are presented, and the relationship between the structure and the thermal properties has also been discussed. The specific heat, anisotropic thermal expansion and thermal conductivity have been carefully measured. The principal thermal expansion and thermal conductivity coefficients have been determined at different temperatures. Thermal expansion of BTM exhibits weak anisotropy though it belongs to low symmetry system. Interestingly, the thermal conductivity of BTM ascends as the temperature is increased.

Introduction

Second-order NLO materials have attracted much attention because of their applications in frequency shifting, optical modulation, and telecommunications and signal processing. Inorganic materials are widely used in these applications due to their high melting point, high mechanical strength, and high degree of chemical inertness. Recently, a variety of strategies have been put forth for creating attractive noncentrosymmetric (NCS) oxide materials by synthesizing inorganic compounds with d^0 transition metal cations (Mo^{6+} or W^{6+}) and cations with nonbonded electron pairs (Se^{4+} or Te^{4+}).[1−13] Both kinds of ions are susceptible to the second-order Jahn−Teller (SOJT) effect, and the influence of a SOJT distortion on the NCS structure was reported by Halasyamani et al.[14] BTM is one of these materials and was first synthesized by Ra et al. through the traditional solid-state reaction method.[11] It crystallizes in a NCS monoclinic crystal system with space group $P2_1$. Its powder SHG efficiency is about 600 × α-SiO_2. Our previous work reported on the bulk crystal growth and optical properties of BTM crystals, and the results indicated that BTM crystal is a preponderant candidate for near−mid-IR nonlinear optical materials.[15] As we know, thermal properties such as thermal expansion, specific heat and thermal conductivity of a crystal will have significant influence on crystal growth and applications.[16,17] If a crystal possesses a large anisotropic thermal expansion, low specific heat and low thermal conductivity, it may be easily cracked during growth and processing if the temperature gradient is too large. The thermal properties can therefore be regarded as important parameters for assessing the possible practical application of a particular crystal.

In this paper, we report the thermal properties of BTM single crystals, including thermal expansion, specific heat and thermal conductivity for the first time. The relationships between structure and thermal properties of BTM are also reported.

Experimental Section

Crystal Growth and Processing. BTM single crystals have been grown by the flux method as we reported previously.[15] Using the seed-testing method, the saturation temperature of the flux system was determined to be about 540 °C. Then, a *b*-oriented seed was dipped into the flux and rotated at 20−40 rpm. The temperature was reduced at a rate of 0.5−1 °C per day as the growth progressed. The period of growth ranged from 40 to 50 days. Figure 1 shows the as-grown BTM crystal. Two cuboid bars with size 4 × 5 × 6 mm^3 and four wafers with size 6 × 6 × 2 mm^3 were cut from this crystal for measuring its thermal properties.

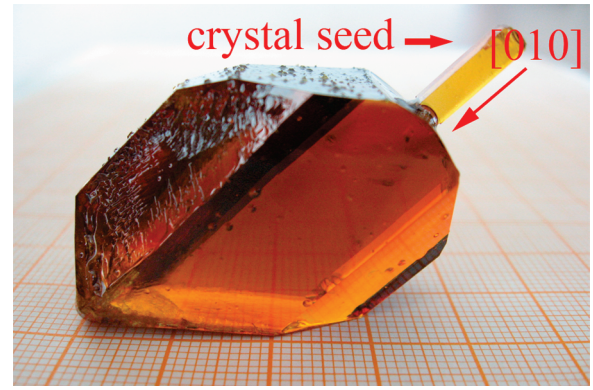

Figure 1. The as-grown bulk BTM crystal. Notice that the crystal owns high optical homogeneity.

Density Measurement. The density of BTM at room temperature (20 °C) had been measured by using the buoyancy method. Some deionized water in a beaker was weighed, and then a bulk BTM crystal hanged by a bit of filament was dipped into the water without touching the bottom of the beaker. After that, the total weight was recorded.

Measurement of the Thermal Properties. The decomposition point of the BTM crystal was measured by thermogravimetry method using Diamond TG/DTA made by the Perkin-Elmer Company in the temperature range from 20 to 1000 °C. Specific heat was measured by the method of differential scanning calorimetry using a simultaneous thermal analyzer (Diamond DSC) made by Perkin-Elmer Company in the temperature range between 20 and 500 °C at a heating rate of 10 K/∼min. The thermal expansion of the BTM crystal was measured with the temperature up to 500 °C by using a thermal dilatometer (Diamond TMA) made by Perkin-Elmer Company. The two crystal bars used for thermal expansion measurements were polished. The thermal diffusion coefficient was measured by the laser flash method using a laser flash apparatus (NETZSCH LFA 447 Nanoflash) in the temperature range from 24 to 300 °C. Four pieces of wafers with the same sizes 6 × 6 × 2 mm^3 having faces perpendicular to *a*, *a**, *b*, and *c** crystallographic directions and coated with graphite on both sides were used to carry out the measurements.

Results and Discussion

Connections of Mo−O Octahedral Group. Since in previous work, the structure of BTM crystal, such as the atomic

* Corresponding author. E-mail address: txt@icm.sdu.edu.cn.

10.1021/cg8011052 CCC: $40.75
Published on Web 04/09/2009

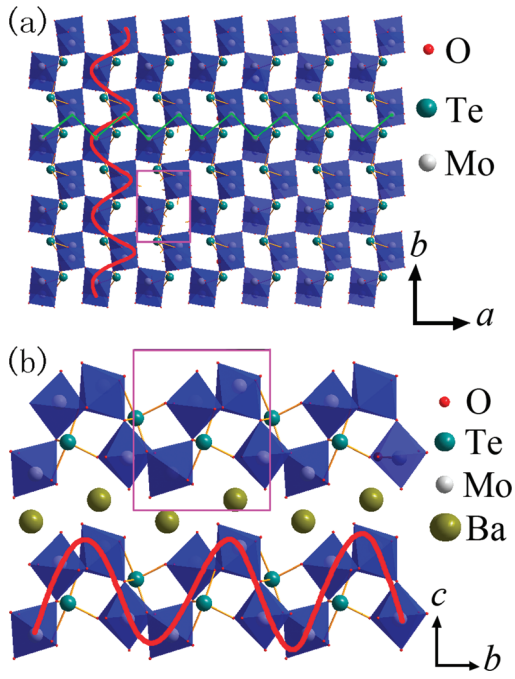

Figure 2. Polyhedral representations of BTM crystal structure in the *ab*-plane (filtrated Ba^{2+} ions) (a) and in the *bc*-plane (b). The green wave and red screws trace the Mo−O polyhedral array along the *a*-axis and the *b*-axis respectively.

positions, bonding lengths and angles, have been discussed in detail,[14,15] here we just focus on the connections of the Mo−O octahedral group, which may present some hints between the structure and the related thermal properties. As shown in Figure 2, parallel to the *b*-axis, there are rigid chains composed of spiral Mo−O octahedra tunnels (see Figure 2 red solenoids) with Te−O polyhedra supporting the screw-pitch. Along the *a*-axis, there are wave-shaped wrinkle structures (see Figure 2 green wave) linked by corner-shared Mo−O octahedra. Along the *c*-axis, there are rigid groups (see Figure 2 pink panes) built up with Mo−O octahedral and Te−O polyhedra which are piled up layer by layer with Ba^{2+} ions occupying the interbedded space as shown in Figure 2(b). The thermal properties of BTM are mainly affected by this its unique structure.

Density. The density of BTM at 20 °C determined by the buoyancy method is 5.4(7) g cm^{-3}, which agrees very well with the calculated value of 5.47(4) g cm^{-3} from the crystallographic data using the formula $\rho = MZ/NV$, where *M* is the molecular weight, *Z* is the number of molecules per unit cell, *N* is Avogadro's number and *V* is the volume of the unit cell. Figure 3 presents the density values at different temperatures calculated through the thermal expansion coefficient. From Figure 3, we can see that the density of BTM crystal linearly decreases as the temperature is increased.

TG/DTA Analysis. To measure the melting point or the decomposition point, thermal gravimetric (TG) and differential thermal analyses (DTA) for the BTM crystal were carried out. The TG/DTA curves of the BTM crystal were given in Figure 4. A single sharp endothermic peak and mass loss were observed at about 602 °C. Before this endothermic peak there are no other endothermic or exothermic peaks, which indicates that for the BTM crystal the decomposition takes place before its melting point and thus it cannot be grown by the Czochralski method.

Specific Heat. For nonlinear optical crystals, the damage threshold and therefore possible applications can be greatly influenced by the specific heat.[17] Figure 5 shows the specific

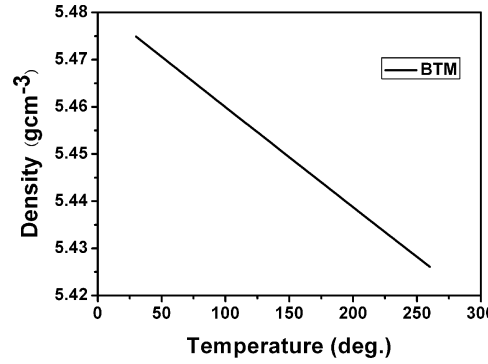

Figure 3. The calculated density vs temperature curve of the BTM crystal.

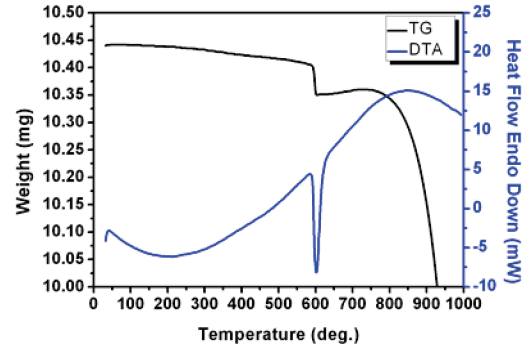

Figure 4. The TG/DTA curves of the BTM crystal. Notice the endothermic peak and mass loss around the temperature 602 °C, which indicates that the BTM crystal decomposed before its melting point.

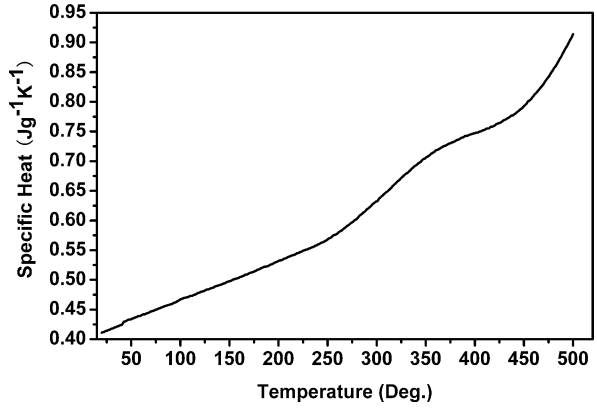

Figure 5. The specific heat vs temperature curve of the BTM crystal.

heat of the BTM crystal varying as a function of the temperature. The specific heat increases almost linearly from 0.41(1) J g^{-1} K^{-1} to 0.91(4) J g^{-1} K^{-1} with the temperature increase from 20 to 500 °C, which means that the BTM crystal can tolerate more thermal energy at high temperature.

Thermal Expansion. For monoclinic BTM crystal the thermal expansion coefficient tensor[18] with respect to the axes in the conventional orientation is

$$\begin{pmatrix} \alpha_{11} & 0 & \alpha_{13} \\ 0 & \alpha_{22} & 0 \\ \alpha_{31} & 0 & \alpha_{33} \end{pmatrix} \quad (1)$$

There are four independent principal thermal components, α_{11}, α_{31} (= α_{13}), α_{22} and α_{33}. In order to determine α_{ij}, we cut

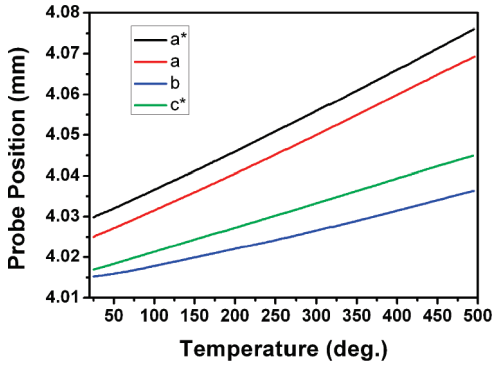

Figure 6. The thermal expansion along different axes of the BTM crystal.

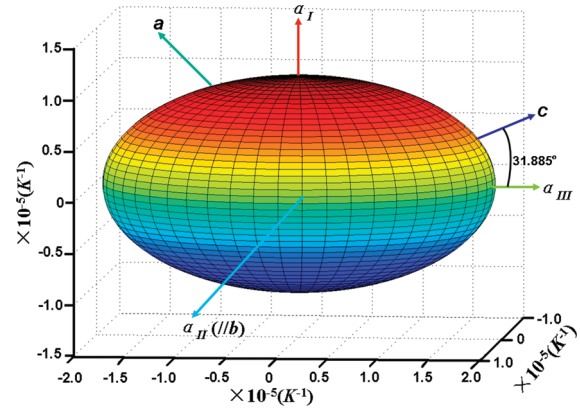

Figure 7. The thermal expansion ellipsoid of BTM crystal.

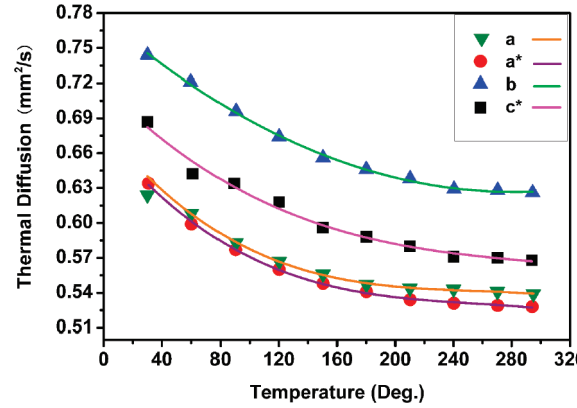

Figure 8. The experimental (symbols) and calculated (solid lines) diffusion coefficients along different axes of the BTM crystal.

samples from the crystal along four different orientations. In the (010) plane, the expansion coefficients corresponding to the three orientations $\xi_1 = 0.89 \pm 0.05°$, $\xi_2 = 90 \pm 0.05°$, and $\xi_3 = 90.89 \pm 0.05°$, measured with respect to the crystallographic *c*-axis, are along the *c**, *a**, and *a* vector directions, respectively. The solid lines in Figure 6 are the thermal expansion ratio curves along the crystallographic axes. It can be seen that the expansion ratio is almost linear over the entire measured temperature range and the BTM crystal exhibits expansion when it is heated. The average linear thermal expansion coefficient for the crystallographic directions can be calculated according to the following formula:

$$\bar{\alpha}(T_0 \rightarrow T) = \frac{\Delta L}{L_0}\frac{1}{\Delta T} \qquad (2)$$

where $\bar{\alpha}(T_0 \rightarrow T)$ is the average linear thermal expansion coefficient over the temperature range of T_0 to T, L_0 is the sample length at T_0, ΔL is the length change when the temperature changes from T_0 to T, and the temperature change is $\Delta T = T - T_0$.

The values of the average linear thermal expansion coefficients of the BTM crystal over the temperature range of 20 to 500 °C are $\alpha_{c^*} = 13.0(5) \times 10^{-6}$ K^{-1}, $\alpha_{a^*} = 16.8(4) \times 10^{-6}$ K^{-1}, $\alpha_a = 16.7(1) \times 10^{-6}$ K^{-1}, and $\alpha_b = 9.2(3) \times 10^{-6}$ K^{-1} respectively. By using the related equations presented in previous references,[18,19] the three coefficients α_{11}, α_{31} and α_{33} were calculated to be $16.8(4) \times 10^{-6}$ K^{-1}, $3.9(7) \times 10^{-6}$ K^{-1} and $12.9(3) \times 10^{-6}$ K^{-1}, respectively. In addition, the expansion coefficient α_{22} in the direction of the crystallographic *b*-axis has also been determined as $9.2(3) \times 10^{-6}$ K^{-1}. For monoclinic BTM crystal, the principal expansion coefficients α_I, α_{II} and α_{III} are calculated to be $10.4(6) \times 10^{-6}$ K^{-1}, $9.2(3) \times 10^{-6}$ K^{-1} and $19.3(1) \times 10^{-6}$ K^{-1}, respectively. The orientation of the principal axis φ is calculated to be 31.885°, which is the angle measured counterclockwise from the α_{III}-axis toward the crystallographic *c*-axis (the α_{II}-axis coincides with the *b*-axis). The relationship between crystallographic orientation and the conventional orientation is demonstrated in Figure 7. The thermal expansion value can be appropriately explained based on its unique crystal structure. Parallel to the *b*-axis, the rigid helical chains composed of spiral Mo−O octahedra tunnels with Te−O polyhedra supporting the screw-pitch are little sensitive to the temperature fluctuating, so the thermal expansion coefficient along the *b*-axis is the smallest one ($\alpha_b = 9.2(3) \times 10^{-6}$ K^{-1}). Along the *a*-axis, the wave-shaped wrinkle structures linked by corner-shared Mo−O octahedra are more susceptible to temperature fluctuation, so the thermal expansion coefficient along the *a*-axis is the largest one ($\alpha_a = 16.7(1) \times 10^{-6}$ K^{-1}). Along the *c*-axis, the rigid groups built up with Mo−O octahedra and Te−O polyhedra piled up layer by layer should have owned small thermal-expansion, but Ba^{2+} ions occupying the interbanded space disturb the compact accumulation of the rigid groups, therefore, the medial thermal expansion value along the *c*-axis is in the middle of the three directions ($\alpha_c \approx \alpha_{c^*} = 13.0(5) \times 10^{-6}$ K^{-1}).

Although the thermal expansion coefficients of the BTM crystal are larger than other monoclinic crystals such as BiB_3O_6,[20] the weak anisotropy of the thermal expansion effectively protects the crystal from cracking caused by thermal expansion during crystal growth, processing and applications.

Thermal Conductivity. The thermal conductivity *k* can be calculated using the following equation:

$$\kappa = \lambda \rho C_p \qquad (3)$$

where *k*, λ, ρ, and C_p denote the principal thermal conductivity, thermal diffusion coefficient, density and specific heat of the crystal, respectively. The thermal diffusion coefficients of the BTM crystal were measured directly along the *a*, *a**, *b*, and *c** directions respectively, and the results are shown in Figure 8. Thus, the thermal conductivity along the directions was calculated according to eq 2, and the data are shown in Figure 9. The thermal conductivity $[k_{ij}]$ of a crystal is also a symmetrical second-rank tensor. In the principal coordinate system, the $[k_{ij}]$ tensor is diagonal like the thermal expansion coefficient tensor. So, we calculated the principal axis (*X*, *Y*, and *Z*) thermal conductivity coefficients at different temperatures similarly to what was done with the thermal expansion coefficients. Table 1 lists the calculated principal axis parameters at different

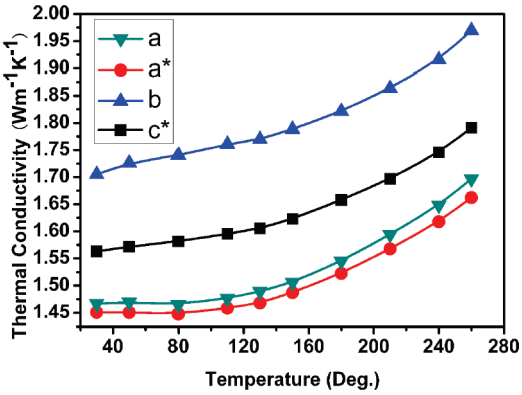

Figure 9. The calculated thermal conductivity in a single BTM crystal.

Table 1. The Principal Axis Parameters of Thermal Conductivity, *X*, *Y*, *Z*, and φ at Different Temperatures

T (°C)	X (W m^{-1} K^{-1})	Y (W m^{-1} K^{-1})	Z (//b) (W m^{-1} K^{-1})	φ (deg)
30	1.2(3)	1.7(9)	1.7(0)	39.2(5)
50	1.2(1)	1.8(2)	1.7(3)	39.7(9)
70	1.2(1)	1.8(4)	1.7(3)	39.5(3)
90	1.2(0)	1.8(5)	1.7(4)	38.6(5)
110	1.2(4)	1.8(2)	1.7(6)	38.7(6)
130	1.2(0)	1.8(9)	1.7(7)	39.6(8)
150	1.2(5)	1.8(7)	1.7(9)	39.1(3)
180	1.2(3)	1.9(6)	1.8(2)	40.1(2)
210	1.2(1)	2.0(7)	1.8(6)	41.0(9)
240	1.2(0)	2.1(8)	1.9(2)	41.7(0)
260	1.1(8)	2.2(9)	1.9(7)	42.1(1)

temperatures. The orientation angle φ of the principal axes is the counterclockwise angle measured from the *Y*-axis to the crystallographic *c*-axis (the *Z*-axis coincides with the *b*-axis). From Figure 9, we can see that the thermal conductivity of the BTM crystal is ascending as the temperature is increased. That is different from other monoclinic crystals such as doped $KLu(WO_4)_2$[21] and $Ca_4YO(BO_3)_3$.[22] This phenomenon indicates that the BTM crystal can tolerate more thermal load at high temperature.

Conclusion

The connections of the Mo−O octahedral group are presented, and the relationship between the structure and the thermal properties has also been discussed. The thermal properties of single crystal BTM were carefully studied by measuring the decomposition point, thermal expansion, specific heat, thermal diffusion coefficient and thermal conductivity. The calculated average principal expansion coefficients α_I, α_{II} and α_{III} are 10.4(6) × 10^{-6} K^{-1}, 9.2(3) × 10^{-6} K^{-1} and 19.3(1) × 10^{-6} K^{-1}, respectively. The BTM crystal possesses relatively large thermal expansion but exhibits weak anisotropy. The thermal conductivity ascends as the temperature is increased; such a phenomenon is uncommon in the monoclinic system and is related to the unique crystal structure of the BTM crystal.

Acknowledgment. This work is supported by the State National Natural Science Foundation of China (Grants 50590403, 50721002) and the 973 program of the People's Republic of China (Grant 2004CB619002).

References

(1) Harrison, W. T. A.; Dussack, L. L.; Jacobson, A. J. *Inorg. Chem.* **1994**, *33*, 6043.
(2) Harrison, W. T. A.; Dussack, L. L.; Jacobson, A. J. *J. Solid State Chem.* **1995**, *120*, 112.
(3) Harrison, W. T. A.; Dussack, L. L.; Jacobson, A. J. *J. Solid State Chem.* **1996**, *125*, 234.
(4) Balraj, V.; Vidyasagar, K. *Inorg. Chem.* **1998**, *37*, 4764.
(5) Halasyamani, P. S.; Poeppelmeier, K. R. *Chem. Mater.* **1998**, *10*, 2753.
(6) Porter, Y.; Ok, K. M.; Bhuvanesh, N. S. P.; Halasyamani, P. S. *Chem. Mater.* **2001**, *13*, 1910.
(7) Welk, M. E.; Norquist, A. J.; Arnold, F. P.; Stern, C. L.; Poeppelmeier, K. R. *Inorg. Chem.* **2002**, *41*, 5119.
(8) Goodey, J.; Broussard, J.; Halasyamani, P. S. *Chem. Mater.* **2002**, *14*, 3174.
(9) Porter, Y.; Halasyamani, P. S. *J. Solid State Chem.* **2003**, *174*, 441.
(10) Goodey, J.; Ok, K. M.; Broussard, J.; Hofmann, C.; Escobedo, F. V.; Halasyamani, P. S. *J. Solid State Chem.* **2003**, *175*, 3.
(11) Ra, H.-S.; Ok, K. M.; Halasyamani, P. S. *J. Am. Chem. Soc.* **2003**, *125*, 7764.
(12) Hou, J. Y.; Huang, C. C.; Zhang, H. H.; Tu, C. Y.; Sun, R. Q.; Yang, Q. Y. *J. Mol. Struct.* **2006**, *785*, 37.
(13) Chi, E. O.; Ok, K. M.; Porter, Y.; Halasyamani, P. S. *Chem. Mater.* **2006**, *18*, 2070.
(14) Halasyamani, P. S.; Poeppelmeier, K. R. *Chem. Mater.* **1998**, *10*, 2753.
(15) Zhang, W. G.; Tao, X. T.; Zhang, C. Q.; Gao, Z. L.; Zhang, Y. Z.; Yu, W. T.; Cheng, X. F.; Liu, X. S.; Jiang, M. H. *Cryst. Growth Des.* **2008**, *8*, 304.
(16) Hou, W. B.; Xu, D.; Yuan, D. R.; Liu, M. G.; Zhang, N.; Tao, X. T.; Sun, S. Y.; Jiang, M. H. *Cryst. Res. Technol.* **1994**, *29*, 939.
(17) Xu, D.; Zhang, K. C.; and Zhang, L. H. *Science and Technology of Crystal Growth*; Science: Beijing, 1997 (in Chinese).
(18) Krishnan, R. S.; Srinivasan, R.; Devanarayanan, S. *Thermal Expansion of Crystals*; Pergamon: Oxford, 1979.
(19) Liu, X. J.; Wang, Z. Y.; Wang, X. Q.; Zhang, G. H.; Xu, S. X.; Duan, A. D.; Zhang, S. J.; Sun, Z. H.; Xu, D. *Cryst. Growth Des.* **2008**, *8*, 2270.
(20) Teng, B.; Wang, J. Y.; Wang, Z. P.; Hu, X. B.; Jiang, H. D.; Liu, H.; Cheng, X. F.; Dong, S. M.; Liu, Y. G.; Shao, Z. S. *J. Cryst. Growth* **2001**, *233*, 282.
(21) Zhang, J. X.; et al. *Appl. Phys. Lett.* **2005**, *87*, 061104.
(22) Ge, W. W.; Zhang, H. J.; Wang, J. Y.; Jiang, M. H.; Sun, S. Q.; Ran, D. G.; Xia, H. R.; Boughton, I. R. *J. Appl. Crystallogr.* **2007**, *40*, 125.

CG8011052